

THIN AEROFOILS OSCILLATING IN A CONFINED INVISCID FLOW

MOURAD Jihad[1], FERRAND Valerie[1] & GOWREE Erwin[1]

[1]ISAE-Supaero

Abstract

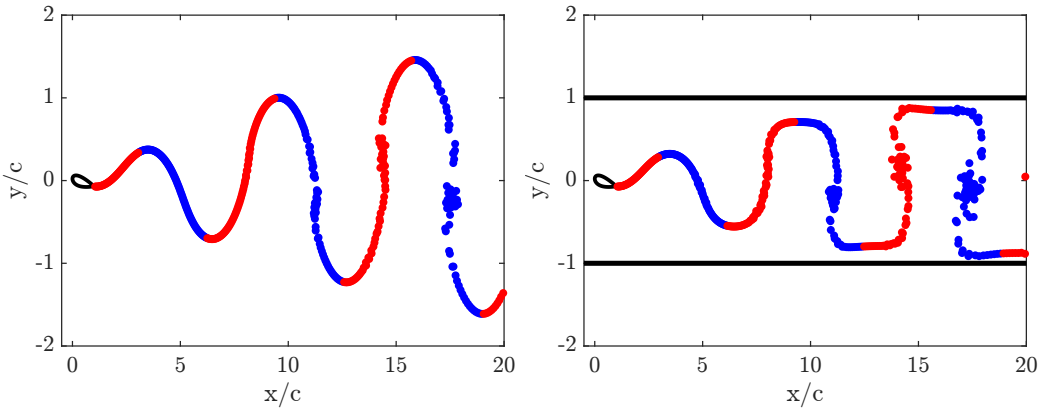
Wake dynamics is an area of interest in plethora of applications specially in confined environments such as that of propulsion or even blockage correction in wind-tunnel testing. This is investigated using a time-marching potential flow model. Two effects are considered: solid confinement due to walls, and confinement caused by the wake dynamics of the upstream oscillating aerofoils. The numerical model is validated against experimental measurements obtained from a simplified wind-tunnel set-up consisting of two parallel aerofoils which can oscillate independently, where good agreement between the numerical and experiment methods is visualised in both temporal evolution and spectral characteristics of the induced angle (α_{ind}) picked up downstream. A parametric study is conducted to assess the influence of forcing frequency, oscillation amplitude, and geometric configuration on wake development and flow response. Spectral analysis shows that when the wake impinged on a third aerofoil positioned along the symmetry plane and downstream of the two parallel aerofoils, the response of the trailing aerofoil was dominated by the harmonic content, whereas interharmonics arise when the wake is modulated, either through wall proximity or wake–wake interactions (wake periodicity has changed). This change in the spectral response is crucial when dealing with aero-elastic or aero-acoustic applications as the transfer of energies between modes in the flow can have either a constructive or destructive impact.

Keywords: Confinement, Wake-Crossing, Distribution

1. Introduction

Confinement effects arise in a variety of applications. In aerospace propulsion systems, confinement is inherent to the flow within ducts and is often desirable. In contrast, in wind-tunnel testing, confinement can limit experimental accuracy due to blockage effects. Wind-tunnel experiments are widely regarded as one of the most reliable approaches for evaluating aerodynamic performance. However, when the test geometry occupies a significant portion of the test section, blockage effects can introduce discrepancies between measured performance and free-flight conditions. These discrepancies arise because the tunnel walls restrict the effective cross-sectional area, leading to flow acceleration in accordance with Bernoulli's principle. A numerical framework capable of predicting these effects can assist in optimising test configurations and reducing confinement-induced discrepancies. Several methods have been proposed in the literature to account for confinement, including the Mirror method [1], Maskell's method [2], and the wall-pressure signature method [3]. However, these approaches present limitations in the context of the present work. Maskell's method [2] is not directly applicable due to the inherently two-dimensional nature of the current numerical capability, while the wall-pressure signature method [3] requires experimental data for extrapolation. Furthermore, the mirror method [1] becomes computationally inefficient when multiple aerofoils are considered in the framework, as it significantly increases the number of mirrored aerofoils, thereby reducing the efficiency of potential flow solvers. To address these limitations, an alternative approach, referred to here as the Solid method, is proposed. This method models wind-tunnel walls as flat plates enforcing a no-penetration condition, thereby confining the flow without requiring an array of images. A similar

approach has been reported by [4] in the context of modelling permeable wind-tunnel walls. The implementation of this method is described in detail in §2.2. The objective of this work was to develop a numerical tool to support the design of a gust generator rig in the ISAE-SUPAERO's wind-tunnel. However, during validation of the model, a deformation was observed in both the numerical and experimental induced angle (α_{ind}) signals. This behaviour, typically associated with viscous effects, was unexpected within the context of an inviscid formulation. In contrast to previous studies, where gust generator models were often formulated in the frequency domain, resulting in idealised wake behaviour and purely sinusoidal responses [5, 6]. The present time-marching approach captures wake convection and its dynamics downstream (see figure 1). This observation motivated a more detailed investigation, leading to the identification of two distinct forms of confinement within the gust generator configuration: solid confinement due to the wind-tunnel walls, and confinement due to the dynamics of the wake, resulting from the wake vortices shed by the oscillating aerofoils surrounding the probe or the downstream aerofoil (see figure 2). Consequently, the scope of the study was extended beyond numerical model validation, to include a systematic investigation of the parameters governing said effects, which includes location of the downstream aerofoil, spacing between the upstream oscillating aerofoils, forcing frequency, and oscillation amplitude. This shift in focus was motivated by the observation of signal deformation in both numerical and experimental results. Such deformations indicate a redistribution of energy within the flow, which may lead to constructive or destructive interactions when coupled with aero-elastic or aero-acoustic phenomena. This highlights the importance of accurately characterising confinement effects, not only for aerodynamic performance but also for their potential impact on coupled physical systems.



(a) Unconfined (b) Confined

Figure 1 – Wake Modelling

2. Methods

2.1 Unsteady Aerofoil Modelling

The numerical solver employed is a time-marching potential flow model, in which the flow is assumed to be irrotational, incompressible, and inviscid. Given the extensive body of literature detailing potential flow theory, only a concise overview is provided here; relevant references are cited at the end of this section. Furthermore, the numerical model used in this study is based on an open-source implementation that has been further extended to meet the requirements of the present research. For a comprehensive description of the original model, the reader is referred to [7]. This section outlines the fundamental principles underlying the potential flow model, along with the specific modifications introduced. The formulation is based on the Laplace equation (see equation 1), subject to several boundary conditions. First, the Neumann boundary condition enforces the impermeability of the body surface (see equation 2). Second, the Kutta condition is imposed to ensure that the flow remains attached to the body and leaves the trailing edge smoothly. The way the Kutta condition is enforced is by assuming that the total vorticity at the trailing edge sums to zero, which is done to the sum of the circulation of the vortices at the first, last panel, and that of the wake panel from which a wake vortex is shed at each time step (see equation 3). Finally, Kelvin's theorem states that circulation around a

closed contour remains constant for inviscid flow with conservative body forces (see equation 4). The primary modifications made to the original code of [7] include the introduction of multiple aerofoils within the numerical domain, as well as the implementation of confinement effects. The treatment of confinement will be detailed in the following section. When multiple aerofoils are present, care must be taken to ensure that Kelvin's theorem is satisfied. This requirement is enforced by ensuring that the sum of the bound and wake vortex strengths associated with each individual aerofoil is zero. This condition is applied consistently to all aerofoils in the domain visualised in figure 2. [8] [9]

$$\nabla^2 \Phi = 0 \tag{1}$$

$$\nabla \phi(x_s,t) + u_m(x_s,t) \cdot n(x_s) = 0 \tag{2}$$

$$\gamma_1(t_k) + \gamma_{n+1}(t_k) + \gamma_{wp} = 0 \tag{3}$$

$$\frac{D\Gamma}{Dt} = 0 \tag{4}$$

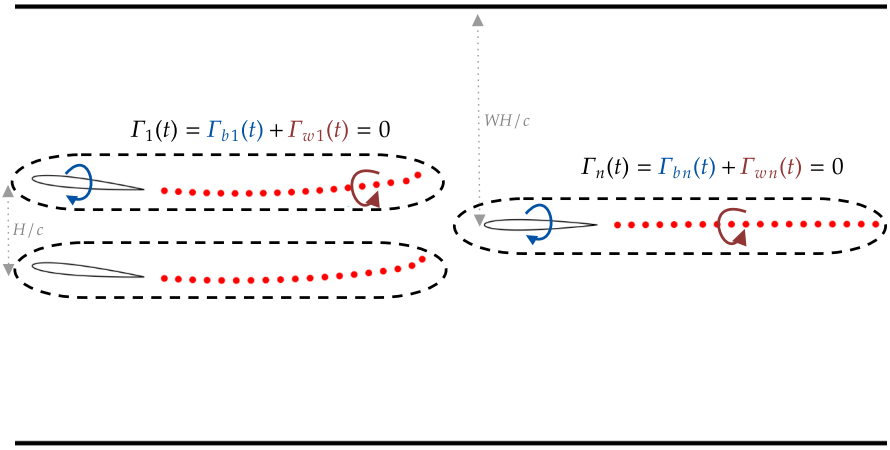


Figure 2 – Numerical Representation of Gust Generator

2.2 Solid Confinement Modelling

The modelling of confinement in the present work differs from the approach commonly adopted in the literature. Typically, confinement effects, such as ground effect or that of wind-tunnel walls, are represented by the mirror method [1]. In this approach, the ground or tunnel walls are treated as lines of symmetry, and both the aerofoil and its wake are reflected about these lines to account for the wall-induced flow modifications. While this method has proven to be effective, its application becomes computationally inefficient when multiple aerofoils are considered. To address this limitation, the confinement in the present study is modelled by representing the walls as stationary flat plates, through which neither the flow nor the wake is permitted to penetrate. This treatment follows a similar approach to that described in the previous section, where the Neumann boundary condition is applied to enforce the impermeability of the boundary. An illustrative case is presented in figure 1, highlighting the modulation of the wake due to the presence of the walls. This modulation affects not only the geometry of the wake but also the convection velocity of the vortices, the implications of these changes on the flow physics will be discussed in detail in subsequent sections. The flat plates representing the walls are treated as stationary steady surfaces; consequently, no wake is shed from their trailing edges.

2.3 Experimental Setup

The experiments were carried out in ISAE-Supaero's open-loop wind-tunnel, which has a test section measuring $50 \times 50 \times 80cm$. All tests were performed at a chord-based Reynolds number of $70,000$. Two NACA 0012 aerofoils, each with a chord length of $10cm$, were mounted symmetrically at $5cm$ above the tunnel centerline. A two component hot-wire probe was positioned 7 chords downstream of the oscillating aerofoils and along the symmetry plane to capture the induced longitudinal and normal velocities (u_{ind} and v_{ind} respectively). Additionally, a pitot-static tube was placed at the inlet to monitor the flow velocity within the test section. A schematic replicating the configuration seen in the wind-tunnel is shown in figure 2.

3. Wake Dynamics

The validation process begins with an analysis of the temporal evolution and spectral characteristics of the induced angle in comparison with experimental measurements. In addition, for a better understanding of the change in the wake dynamics due to confinement, an aerofoil will be placed downstream with its location along the centerline varied; furthermore, the spacing between the two oscillating aerofoils will be varied as well ('H/c' see 2). This is done to showcase the impact of the blockage caused by the wake on the flow with respect to the frequency and amplitude of oscillation.

3.1 Temporal

Before examining in detail the salient features, the model demonstrates satisfactory agreement with the experiment seen across all subfigures in figure 3. The observed phase shift can be attributed primarily to viscous effects, as the model is based on an inviscid formulation, as discussed in the methods section. Additionally, the experimental flow is not strictly two-dimensional due to the configuration and placement of the oscillating wing, where there was a gap between the tips of the wing and the tunnel walls, which introduces three-dimensional effects. In particular, the three-dimensional nature of the flow predominantly influences the magnitude of the induced angle. This behaviour is further supported by the observation that the discrepancy in magnitude between numerical and experimental results increases with increasing oscillation amplitude. As the oscillation amplitude increases, the vortex spillage becomes more significant, enhancing the associated downwash and reducing the effective aerodynamic loading due to three-dimensional effects. Before proceeding further with the validation of the numerical results, it is also worth noting that, as the frequency of oscillation increases, the influence of confinement becomes less pronounced.

Focusing now on the signal's characteristics, it is observed that at lower frequencies of the oscillating aerofoils, the measured signals exhibit a relatively high level of noise, seen in figures 3a, 3e, 3i, 3m. However, as the forcing frequency increases, the signal becomes progressively cleaner, facilitating a clearer comparison between numerical and experimental results. An additional feature of interest, which to the authors' knowledge has not been extensively reported in the literature (since most similar interpretation of the numerical method reported in the literature, solve the wake in the frequency domain, resulting in its horizontal convection, limiting the effect of the wake crossing the probe), is the deformation of the signal associated with the passage of wake vortices across the location of the probe. This phenomenon is clearly visible in the numerical and experimental signals, for example, in cases with $\theta = 7^\circ$ and 8° at higher forcing frequencies, shown in figures 3l, and 3p. It is also noteworthy that the modelling approach adopted for confinement reproduces waveforms consistent with experimental observations. As expected, confinement restricts the flow field within the domain (see figure 1b), thereby limiting wake motion relative to an unconfined case. Figure 3k the unconfined configuration signal exhibits noticeable deformation, whereas in the confined case the signal remains comparatively regular, in agreement with experimental observations. For clarity, the reader is referred to the figures corresponding to a forcing frequency of $8\mathrm{Hz}$ and oscillation amplitudes of 7° and 8°, which are figures 3l and 3p, providing a clear illustration of what is meant by a signal's shape deforming.

3.2 Spectral

Since the numerical model captures the deformation of the signal associated with the passage of wake vortices across the probe, a spectral analysis is performed to identify the frequencies excited

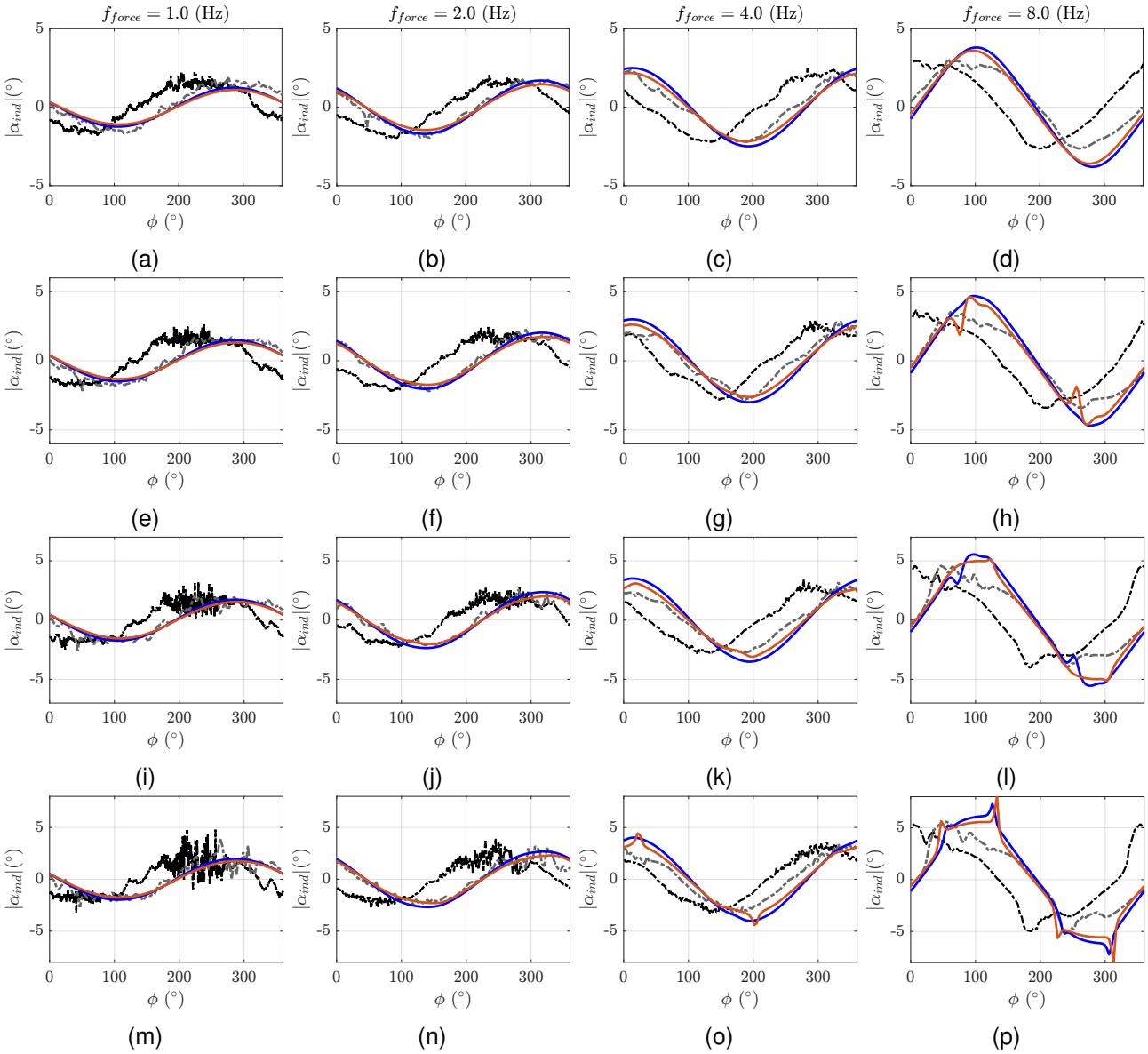


Figure 3 – $\alpha_{induced}$ vs ϕ: (a)-(d) $\theta = 5^\circ$, (e)-(h) $\theta = 6^\circ$, (i)-(l) $\theta = 7^\circ$, (m)-(p) $\theta = 8^\circ$; Exp, Exp-Shifted, Confined, Unconfined

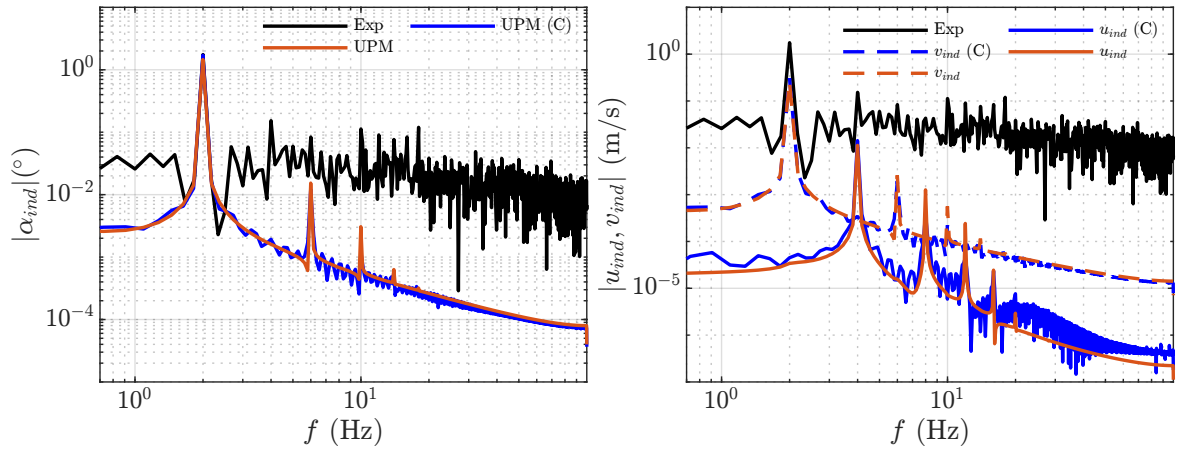
by this phenomenon. Three representative cases are selected for this analysis, as shown in figure 4. The comparison is conducted by analysing the spectra of the numerically obtained induced angle signal (α_{ind}) alongside the experimental measurements, seen in first column of figure 4. In addition, for each case, the spectral content of the experimental gust signal is compared with that of the induced longitudinal and normal velocity components at the probe location (u_{ind} and v_{ind} respectively), seen in second column of figure 4. This approach enables validation that the dominant harmonics identified experimentally are also captured numerically. For the first case (figure 4a), corresponding to $f = 2\text{Hz}$ and $\theta = 5^\circ$, both numerical configurations capture the first three odd harmonics. The confined case additionally exhibits interharmonics, which are attributed to wake modulation induced by confinement (this will be examined further in subsequent subsections). Although the relevant temporal signal shown in figure 3b does not show significant differences between the confined and unconfined configurations, confinement alters the convection speed of the vortices, leading to the emergence of interharmonics in the spectra. Furthermore, figure 4b demonstrates that the dominant harmonic content observed experimentally is recovered in the spectra of the numerically obtained velocity components.

For the second case (figures 4c and 4d), corresponding to $f = 8\text{Hz}$ and $\theta = 2^\circ$, from figure 4c the numerical results exhibit only two dominant peaks in both confined and unconfined configurations. In

contrast, the experimental spectra displays multiple peaks, which can be attributed to viscous effects and also background noise in the wind-tunnel. As noted previously, the influence of confinement decreases with increasing frequency, which is reflected here by the similarity of the confined and unconfined spectra. No interharmonics are observed, as the wake is only weakly modulated by the walls due to the oscillation amplitude being relatively small. The wake trajectory is therefore primarily governed by the imposed pitching motion. As in the previous case, figure 4d shows that the dominant experimental peaks are captured by the spectra of the induced velocity components.
For the final case corresponding to $f = 8\text{Hz}$ and $\theta = 8^\circ$, (figures 4e and 4f), similar overall trends are observed; however, an important distinction is that both confined and unconfined configurations exhibit interharmonics. The presence of interharmonics in both configurations, despite earlier observations linking them primarily to wake-wall modulation, can be explained by wake–wake interactions. At high oscillation amplitude and frequency, the wakes generated by the oscillating aerofoils interact strongly and modulate each other, altering the periodicity of the flow relative to that of an isolated aerofoil. In the confined configuration, the wake is subject to additional modulation due to the presence of the walls.
Based on the results presented, the numerical approach can be considered to be reliable in its ability to capture the dominant spectral features of the flow. To further attribute the observed spectral peaks and distinguish between the different confinement mechanisms, a systematic analysis is subsequently undertaken. This involves, first, by replacing the probe with a aerofoil along the centreline and varying its position relative to the wake. Second, examining the influence of geometric confinement by varying the spacing between the upstream oscillating aerofoils. The parameter that will be considered from this point onwards in the report is the coeffcient of lift of said aerofoil (C_L), no longer the induced angle.

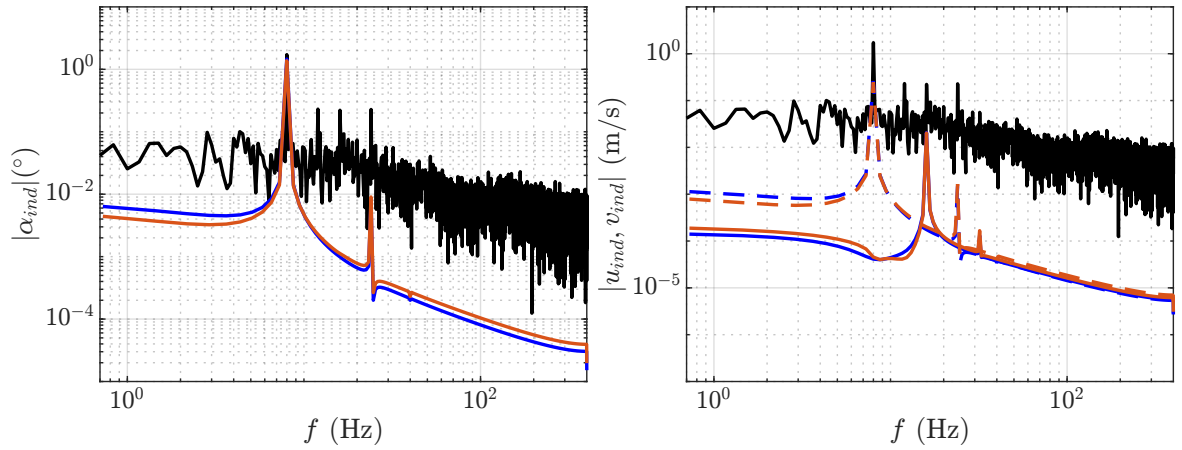
3.3 Aerofoil Position

To further validate the reason behind the amplitudes picked up for the harmonic and interharmonic frequencies identified in the previous spectral analysis, the impact of the wake on an aerofoil positioned downstream is investigated. Its position is varied along the centreline between the two oscillating aerofoils, as shown in figure 5. From first row of figure 6, it can be observed that at a forcing frequency of $f = 2\text{Hz}$ the harmonic content is negligible when the aerofoil is located close to the oscillating aerofoils seen in figure 6a. This is because, in this configuration, the wake does not intersect the aerofoil, as illustrated in figures 5a and 5b. For most configurations in 2Hz, the wake does not significantly impinge on the airfoil in the examined locations seen in figures 6b, 6c, 6d, explains the weak appearance of the harmonic content. When the forcing frequency is increased to 8Hz while maintaining the same oscillation amplitude, the harmonic content becomes more energetic as the aerofoil is positioned further downstream, as seen in second row of figure 6. Although there is no direct wake–aerofoil intersection (seen in figures 5c and 5d), the wake is seen to be in closer proximity to the aerofoil, thereby strengthening the presence of the harmonic response. In these cases, the wake is not significantly modulated, neither by confinement nor by wake–wake interaction, which explains the absence of interharmonics.
At the same frequencies, increasing the oscillation amplitude to $\theta = 8^\circ$ results in a further increase in energy in the harmonics. For $f = 2\text{Hz}$, interharmonics remain absent across all aerofoil positions seen across figure 8. This is consistent with the wake visualisations (figures 7a and 7b), which show limited modulation by the confining walls. The increased amplitude enhances the likelihood of wake crossing the aerofoil, thereby strengthening the harmonic components, as reflected in first row of figure 8. The slightly richer harmonic content observed in the unconfined case can be attributed to the more pronounced oscillatory motion of the wake, which increases the occurences of wake–aerofoil crossing, particularly at downstream positions (7 and 16 chords), seen in figures 8c and 8d. Upon increasing the frequency to $f = 8\text{Hz}$ while maintaining $\theta = 8^\circ$, the harmonic content becomes significantly more energetic compared to the corresponding 2Hz case. In the confined configuration, interharmonics are now present across all aerofoil positions, consistent with wake modulation induced by wall proximity, seen in first row of figure 8. In addition, as observed previously, when both the oscillation amplitude and frequency are sufficiently high, wake–wake interactions alone can induce modulation, leading to the appearance of interharmonics even in the absence of walls. This behaviour is particularly evident



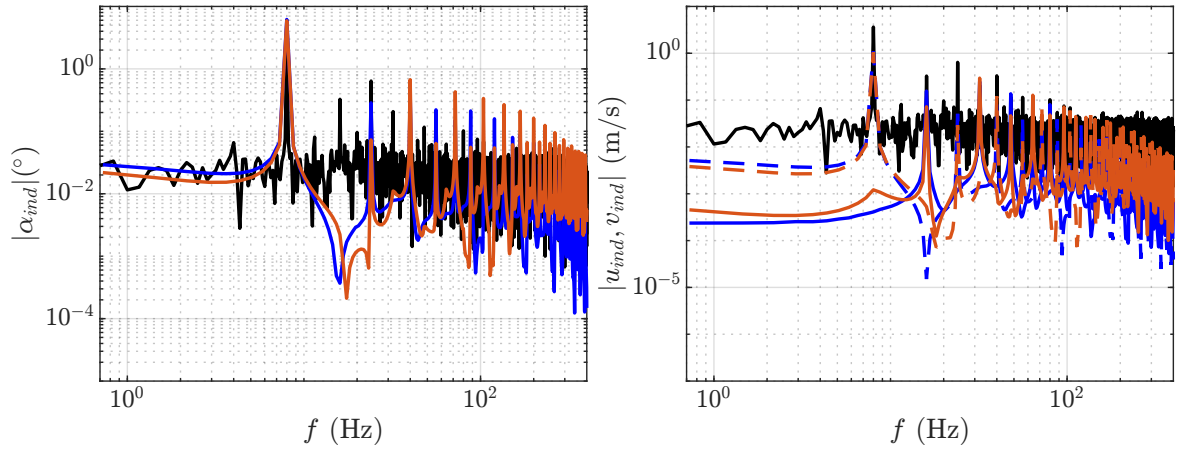
(a) $Freq = 2Hz$ and $\theta = 5^\circ$

(b) $Freq = 2Hz$ and $\theta = 5^\circ$



(c) $Freq = 8Hz$ and $\theta = 2^\circ$

(d) $Freq = 8Hz$ and $\theta = 2^\circ$



(e) $Freq = 8Hz$ and $\theta = 8^\circ$

(f) $Freq = 8Hz$ and $\theta = 2^\circ$

Figure 4 – 1st Column α_{ind} vs frequency, 2nd Column u_{ind}, v_{ind} vs frequency

when the downstream aerofoil is located at 7 and 16 chords as seen in figures 8g and 8h, where the wakes have developed sufficiently to interact and modulate one another. The hypothesis that interharmonics are linked to wake modulation will be investigated further in the following section by increasing the spacing between the two oscillating aerofoils. It is expected that, as the oscillating aerofoils are placed further apart, the wake–wake interactions will weaken, and the corresponding interharmonic content will diminish even at higher frequencies and amplitudes for the unconfined case.

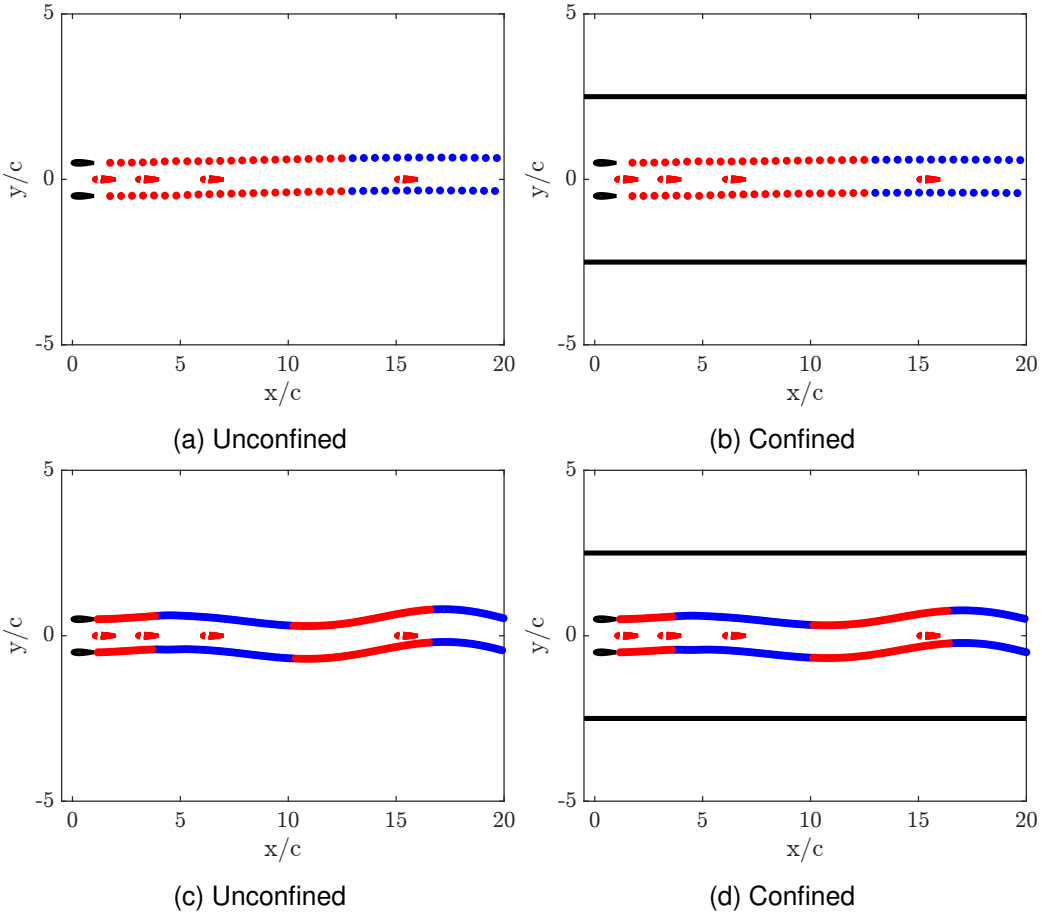


Figure 5 – Wake Dynamics, $\theta = 2°$: (a)-(b) $f_{force} = 2Hz$, (c)-(d) $f_{force} = 8Hz$

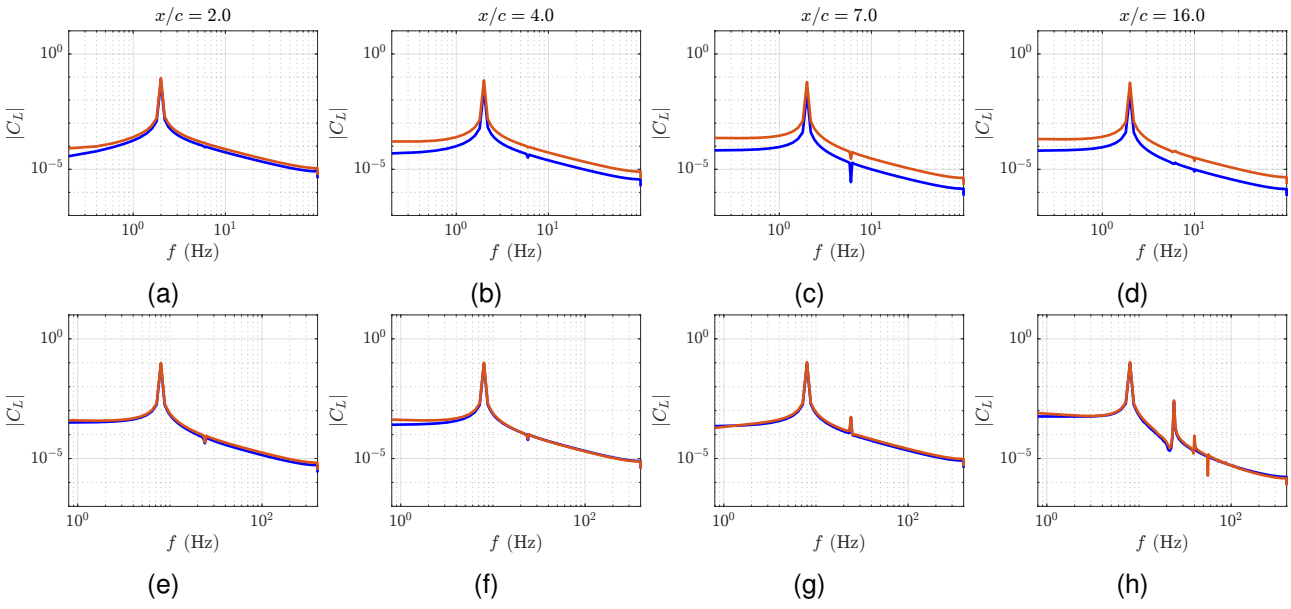


Figure 6 – C_L vs frequency, $\theta = 2°$: (a)-(d) $f_{force} = 2Hz$, (e)-(h) $f_{force} = 8Hz$

3.4 Spacing between the aerofoils

Fixing the downstream aerofoil 7 chords away from the upstream aerofoils, setting the forcing frequencies to $f = 2$ and 8Hz and a fixed oscillation amplitude of $\theta = 2°$, it can be observed from the first row of figure 9 that at $f = 2$Hz the response showcases harmonic components across all cases, with no significant presence of interharmonics (except when the oscillating aerofoils are in the closest proximity to the walls, seen in figure 9d). This is attributed to the absence of prominent wake modu-

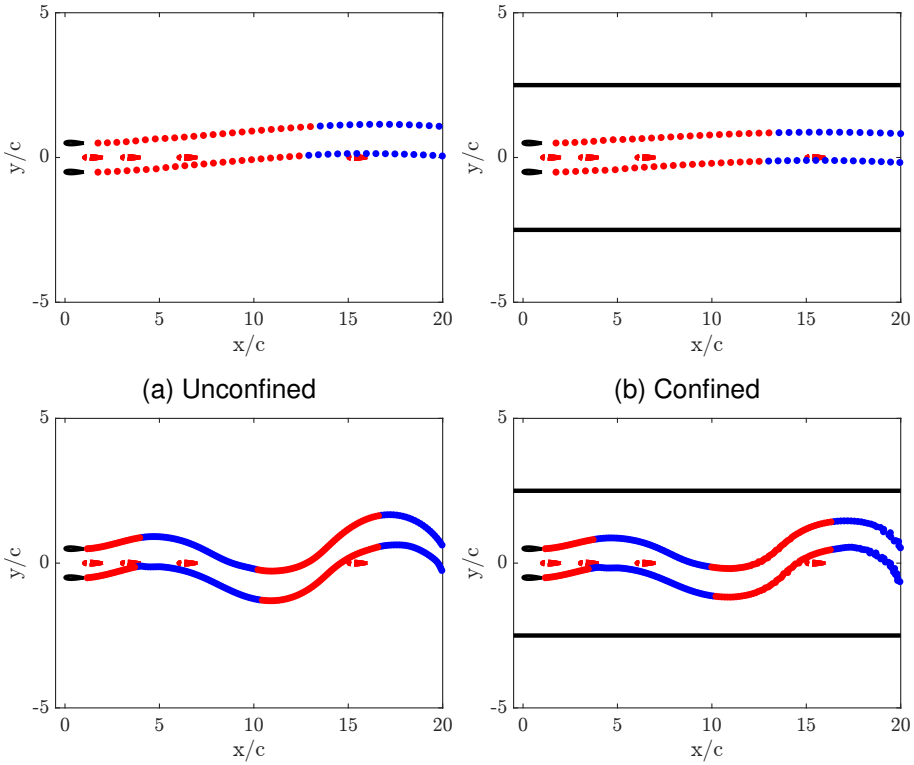


Figure 7 – Wake Dynamics, $\theta = 8°$: (a)-(b) $f_{force} = 2Hz$, (c)-(d) $f_{force} = 8Hz$

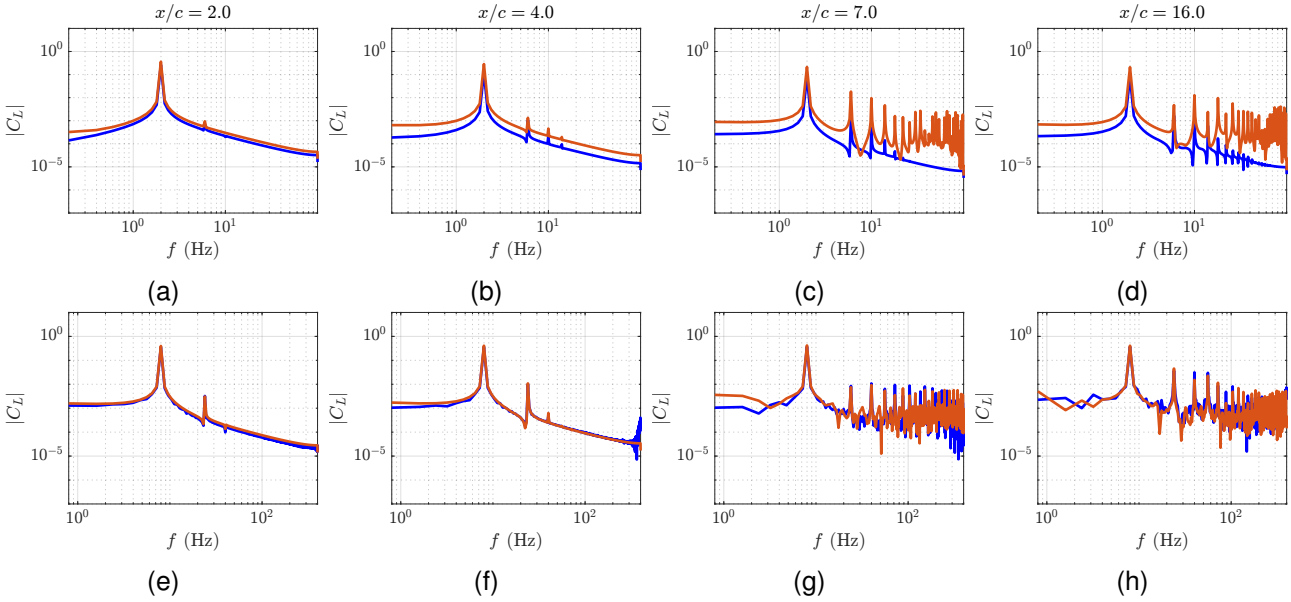


Figure 8 – C_L vs frequency, $\theta = 8°$: (a)-(d) $f_{force} = 2Hz$, (e)-(h) $f_{force} = 8Hz$

lation, either through wake–wake interaction or wake-wall modulation. A key observation, illustrated in figure 9, is that reducing the spacing between the oscillating aerofoils enhances the energy of the harmonic components, as seen in 9d to 9a, due to the fact that the wake from the oscillating aerofoils is in closer proximity to the aerofoil downstream, especially for the unconfined case due to the free wake.

Upon increasing the frequency to $f = 8$Hz, a similar trend is observed in second row of figure 9: decreasing the spacing between the aerofoils leads to increased energy in the harmonic. In addition, as the aerofoils are positioned closer to the walls, the energy associated with interharmonics increases, visualised in figure 9h.

Returning to the case of $f = 2\text{Hz}$ and increasing the oscillation amplitude to $\theta = 8^\circ$ seen in first row of figure 10, interharmonics begin to emerge when the aerofoils are positioned closer to one another, figures 10a and 10b. In this configuration, both harmonic and interharmonic components become more pronounced due to enhanced wake–wake interaction. In contrast, in the unconfined configuration, the wake can convect freely, which promotes stronger wake–wake interaction and leads to a more prominent interharmonic content when the aerofoils are closely spaced. As the spacing is increased (e.g. $H/c = 1.0$ and 2.0, figures 10c and 10d), these interactions weaken, and the interharmonics diminish. For the confined configuration, positioning the aerofoils closer to the walls consistently enhances wake modulation, resulting in the presence of interharmonics. This behaviour contrasts with the unconfined case, where interharmonics are primarily governed by aerofoil spacing and frequency.

At the higher forcing frequency of $f = 8\text{Hz}$ (second row of figure 10), the combined effects become more pronounced. When the aerofoils are spaced far apart, the unconfined configuration exhibits minimal wake modulation and, consequently, negligible interharmonic content. As the aerofoils are brought closer together, interharmonics emerge due to increased wake–wake interaction. In contrast, interharmonics are present across all confined configurations. This reflects the fact that wake modulation is consistently induced, either through wake–wake interaction when the aerofoils are closely spaced, or through wake-wall interaction when they are further apart.

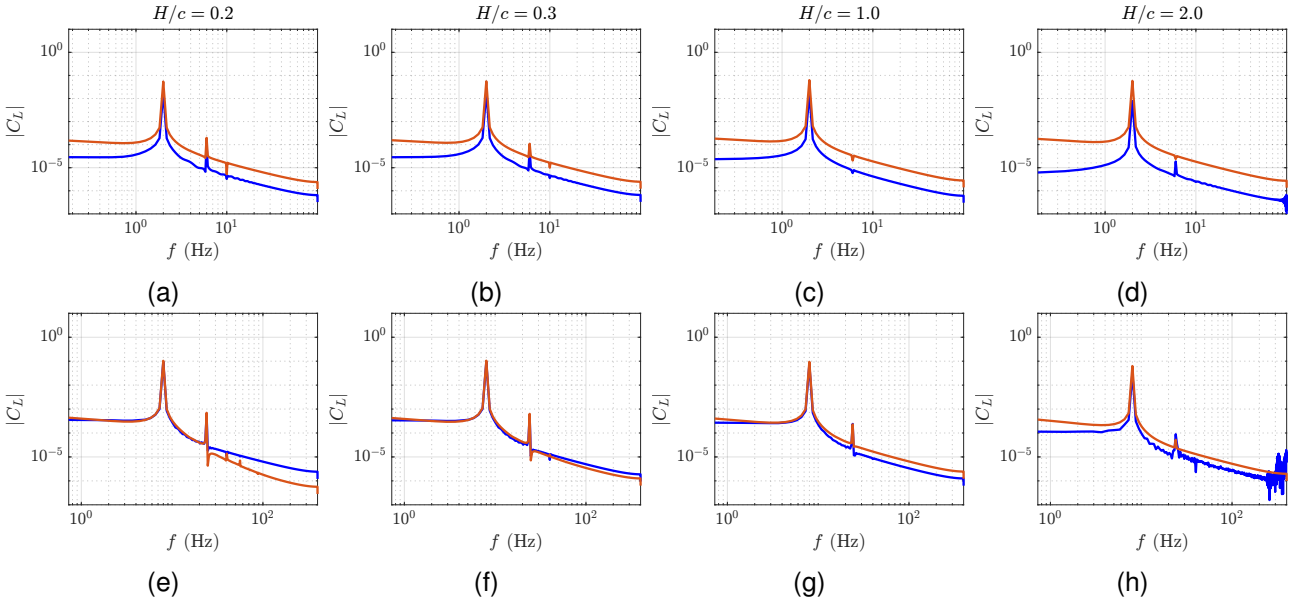


Figure 9 – C_L vs frequency, $\theta = 2^\circ$: (a)-(d) $f_{force} = 2Hz$, (e)-(h) $f_{force} = 8Hz$

4. Conclusion

This study has investigated the impact of confinement on unsteady aerodynamic interactions using a time-marching potential flow model, with particular emphasis on distinguishing between two distinct confinement mechanisms: solid confinement induced by walls and that due to the dynamics of the wake from the upstream aerofoils. The numerical framework was first validated against experimental data, demonstrating good agreement in terms of temporal evolution and spectral characteristics of the induced angle, with discrepancies attributed primarily to viscous and three-dimensional effects absent from the inviscid two-dimensional model. The analysis revealed that the confinement caused by the dynamics of the wake plays a dominant role in determining the flow physics when multiple oscillating aerofoils are present. In such configurations, the interaction and modulation of wakes lead to the emergence of interharmonics in the spectral response. These interharmonics were shown to originate from both wake–wall and wake–wake interactions, with their prominence depending strongly on the oscillation frequency, amplitude, and relative positioning of the aerofoils. As the frequency increases, the influence of confinement diminishes, and the flow becomes increasingly dominated

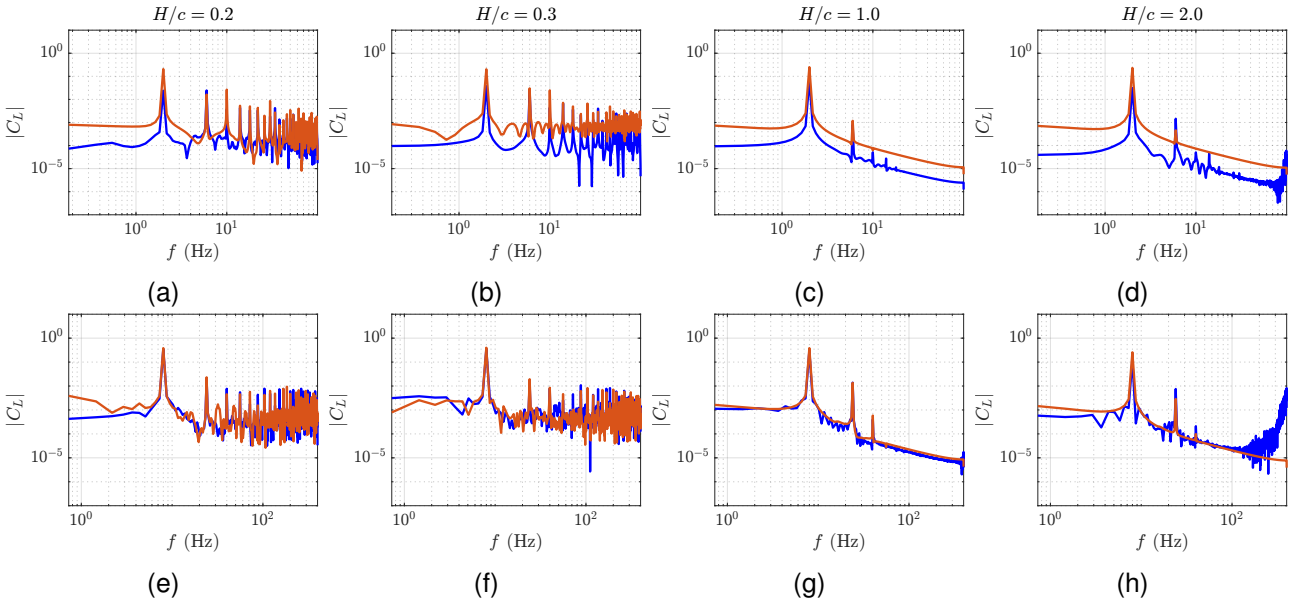


Figure 10 – C_L vs frequency, $\theta = 8°$: (a)-(d) $f_{force} = 2Hz$, (e)-(h) $f_{force} = 8Hz$

by the imposed oscillatory motion. This results in a convergence between confined and unconfined configurations, both in the temporal response and in the spectral content.

5. Contact Author Email Address

The contact author email address should appear explicitly in this section to facilitate future contacts. For example, mailto: jihad.mourad2@isae-supaero.fr.com

6. Copyright Statement

The authors confirm that they, and/or their company or organization, hold copyright on all of the original material included in this paper. The authors also confirm that they have obtained permission, from the copyright holder of any third party material included in this paper, to publish it as part of their paper. The authors confirm that they give permission, or have obtained permission from the copyright holder of this paper, for the publication and distribution of this paper as part of the ICAS proceedings or as individual off-prints from the proceedings.

7. Copyright Statement

$https://doi.org/10.71945/icas2026_0637$

References

[1] H Julian Allen and Walter G Vincenti. Wall interference in a two-dimensional-flow wind tunnel with consideration of the effect of compressibility. Technical report, US Government Printing Office, 1944.

[2] EC Maskell. A theory of the blockage effects on bluff bodies and stalled wings in a closed wind tunnel. 1963.

[3] Binbin Wei, Yongwei Gao, Ruiyang Qiao, and Shuling Hu. A novel wall interference correction method for airfoil. *Advances in Aerodynamics*, 6(1):27, 2024.

[4] William J Devenport, Ricardo A Burdisso, Aurelien Borgoltz, Patricio A Ravetta, Matthew F Barone, Kenneth A Brown, and Michael A Morton. The kevlar-walled anechoic wind tunnel. *Journal of Sound and Vibration*, 332(17):3971–3991, 2013.

[5] H Stapountzis. An oscillating rig for the generation of sinusoidal flows. *Journal of Physics E: Scientific Instruments*, 15(11):1173, 1982.

[6] SF Harding and IG Bryden. Generating controllable velocity fluctuations using twin oscillating hydrofoils. *Journal of Fluid Mechanics*, 713:150–158, 2012.

[7] Grigorios Dimitriadis. *Numerical Incompressible 2D Models*, chapter 4. John Wiley & Sons, 2023.

[8] J. Katz and A. Plotkin. *Low-Speed Aerodynamics*. Cambridge University Press, 2001.

[9] JL Hess and AMO Smith. Calculation of potential flow about arbitrary bodies. *Progress in aeronautical sciences*, 8:1–138, 1967.